INTERNATIONAL JOURNAL FOR NUMERICAL METHODS IN FLUIDS, VOL. 19, 1013–1038 (1994)

# DEVELOPMENT OF PROJECTION AND ARTIFICIAL COMPRESSIBILITY METHODOLOGIES USING THE APPROXIMATE FACTORIZATION TECHNIQUE

A. PENTARIS, K. NIKOLADOS AND S. TSANGARIS

*Laboratory of Aerodynamics, National Technical University of Athens, PO Box 64070, 15710 Zografou, Athens, Greece*

SUMMARY

Predictions for two-dimensional, steady, incompressible flows under both laminar and turbulent conditions are presented. The standard $k$–$\varepsilon$ turbulence model is used for the turbulent flows. The computational method is based on the approximate factorization technique. The coupled approach is used to link the equations of motion and the turbulence model equations. Mass conservation is enforced by either the pseudocompressibility method or the pressure correction method. Comparison of the two methods shows a superiority of the pressure correction method. Second- and fourth-order artificial dissipation terms are used in order to achieve good convergence and to handle the turbulence model equations efficiently. Several internal and external test cases are investigated, including attached and separated flows.

KEY WORDS Navier–Stokes equations Laminar flow Turbulent flow Pseudocompressibility method Pressure correction method Projection method Artificial dissipation

## 1. INTRODUCTION

Many of the fluid flows of practical interest, laminar or turbulent, have one or more recirculation zones, making precise numerical simulation difficult. Numerical models that are capable of accurately predicting such flows are desirable.

Such numerical models consist of a mathematical model and a solution algorithm. The mathematical model comprises the set of differential equations that are solved, algebraic relations and boundary conditions, which include the mass and mean momentum equations, the turbulence model equations, etc. These equations contain approximations, so that the accuracy of the mathematical model has to be tested and verified by comparisons with experimental data or other reliable numerical results for a wide range of test cases. In addition, the solution algorithm, usually a finite volume, finite element or finite difference method, does not give an exact solution, but one involving mathematical inaccuracies. Therefore the final solutions contain errors from two different sources.

Regarding the solution algorithm, the approximate factorization technique is used in the present study. This technique was initially developed for compressible flows[1] but has been successfully used for incompressible flows as well.[2] Regarding the mathematical model, the handling of the mass equation is of most interest. Two alternatives are used. The first is the artificial compressibility method which links the pressure time derivative to the continuity equation. Upon adding the two momentum equations, the numerical algorithm leads to an implicit scheme in time with three equations. Secondly, a pressure correction method is developed

CCC 0271–2091/94/231013–26

*Received February 1994*
*Revised June 1994*

which uses a Poisson equation for the explicit pressure derivation, while the numerical algorithm involves only the momentum equations. A comparison of the above two approaches is one of the aims of the present work.

Concerning the turbulence model, there are plenty of options. The standard $k$–$\varepsilon$ model with the wall function equations was selected because it is well tested and widely used, in spite of its disadvantages. In addition, small values of $y^+$ are not required, so coarse grids can be used near the walls and thus large time steps are possible and fast convergence is obtained. It is expected that this turbulence model will sometimes perform poorly, especially in the recirculation zones.

Another factor that decreases the numerical accuracy is the artificial dissipation terms. These terms, which have to be as small as possible, are required to enhance stability and to remove the oscillations that occur when a central difference scheme is used. In our work a blended non-linear dissipation model is used for the first time in an incompressible algorithm, although it has been applied extensively in compressible algorithms. It was found to be reliable and stable.

## 2. THE TURBULENCE MODEL EQUATIONS

Turbulent flows have been successfully computed over a wide range of flow regimes with the Reynolds-averaged Navier–Stokes equations using the high-Reynolds-number form[3] of the $k$–$\varepsilon$ model. This formulation requires the use of wall functions to bridge the viscous and boundary layers in proximity to the solid wall. This method, in which the influence of the molecular viscosity is not modelled, is strictly valid only for attached shear layers and may perform poorly in the recirculation zones.

The non-dimensional equations of the standard $k$–$\varepsilon$ model are the kinetic energy ($k$) equation

$$\frac{\partial k}{\partial t} + \frac{\partial uk}{\partial x} + \frac{\partial vk}{\partial y} + \alpha \frac{vk}{y} = \frac{1}{Re}\left(\frac{\partial}{\partial x}(\Gamma_k k_x) + \frac{\partial}{\partial y}(\Gamma_k k_y) + \frac{\alpha}{y}(\Gamma_k k_y) + \tilde{G} - Re\ \varepsilon\right)$$

and the dissipation rate ($\varepsilon$) equation

$$\frac{\partial \varepsilon}{\partial t} + \frac{\partial u\varepsilon}{\partial x} + \frac{\partial v\varepsilon}{\partial y} + \alpha \frac{v\varepsilon}{y} = \frac{1}{Re}\left(\frac{\partial}{\partial x}(\Gamma_\varepsilon \varepsilon_x) + \frac{\partial}{\partial y}(\Gamma_\varepsilon \varepsilon_y) + \frac{\alpha}{y}(\Gamma_\varepsilon \varepsilon_y) + C_1 \frac{\varepsilon}{k}\tilde{G} - Re\ C_2 \frac{\varepsilon^2}{k}\right),$$

where $\alpha = 0$ for the two-dimensional equations, $\alpha = 1$ for the axisymmetric equations, $Re$ is the Reynolds number, $\tilde{G}$ is the kinetic energy production term,

$$\tilde{G} = \nu_t\left[2\left(u_x^2 + v_y^2 + \alpha \frac{v^2}{y^2}\right) + (u_y + v_x)^2\right],$$

and

$$\Gamma_k = \frac{\nu_{\text{eff}}}{\sigma_k}, \qquad \Gamma_\varepsilon = \frac{\nu_{\text{eff}}}{\sigma_\varepsilon}, \qquad \nu_{\text{eff}} = \nu_l + \nu_t,$$

with $\nu_{\text{eff}}$ and $\nu_l$ the effective and laminar kinematic viscosity respectively and $\nu_t$ the turbulent kinematic viscosity,

$$\nu_t = Re\ C_\mu \frac{k^2}{\varepsilon}.$$

Finally, the constants are

$$C_1 = 1{\cdot}44, \qquad C_2 = 1{\cdot}92, \qquad C_\mu = 0{\cdot}09, \qquad \sigma_k = 1{\cdot}0, \qquad \sigma_\varepsilon = 1{\cdot}3.$$

The above model is valid under the hypothesis of homogeneous turbulence. It is necessary to avoid solving in the near-wall regions where steep variations and dissipation anisotropy occur. Thus the concept of wall functions has been employed. The central idea is that the flow in the region near the wall can be assumed to behave as a one-dimensional Couette flow. This is a reasonable assumption except for regions of high pressure gradient, separation or reattachment. Once this assumption is made, it is rather easy to arrive at exact or semi-empirical, relations[3] which link the shear stresses and the other variables at the wall to the values of velocity, turbulence energy, etc. at the outer edge of the Couette layer where the first interior grid point is located.

A one-dimensional Couette flow analysis yields, in the absence of a significant pressure gradient, the following linear or logarithmic laws for the distribution of the parallel-to-the-wall velocity $U_P$ at the first grid point P from the wall:

laminar sublayer: $U_P = u^* y^+$ for $y^+ \leqslant 11{\cdot}63$,

turbulent sublayer: $U_P = \dfrac{u^*}{\kappa} \ln(Ey^+)$ for $y^+ > 11{\cdot}63$,

where

$$y^+ = \frac{y}{\nu} u^*$$

is the dimensionless distance of point P from the wall,

$$u^* = \left(\frac{\tau_w}{\rho}\right)^{1/2}$$

is the friction velocity, $\tau_w$ is the wall shear stress, $y$ is the normal distance from point P to the wall, $\kappa = 0{\cdot}4187$ is the Von Karman constant and $E = 9{\cdot}793$ is a roughness parameter.

From the above relations and according to the position of the first point P (laminar or turbulent sublayer), it is possible to calculate the shear stress $\tau_w$.

Finally, assuming that the shear stress is constant in the sublayer, the kinetic energy $k_P$ and dissipation $\varepsilon_P$ at point P are found to be

$$k_P = C_\mu^{-1/2} u^{*2}, \tag{1a}$$

$$\varepsilon_P = C_\mu^{3/4} \frac{k_P^{3/4}}{\kappa y}. \tag{1b}$$

## 3. THE GOVERNING EQUATIONS

### *3.1. The artificial compressibility method*

This approach is designed for steady incompressible flows. As long as the primitive variable formulation (pressure and velocity) is retained for incompressible flows, neither pressure nor

density appears in the continuity equation, with the result that this equation cannot be directly used to compute the pressure field. A pseudo-unsteady form of the continuity equation was proposed by Chorin,[4]

$$\frac{1}{\beta}\frac{\partial p}{\partial t} + \frac{\partial u}{\partial x} + \frac{\partial v}{\partial y} + \alpha\frac{v}{y} = 0,$$

where $\beta > 0$ is the artificial compressibility parameter.

The above equation can be utilized to compute the pressure field. However, since mass conservation is enforced only at the steady state, it is impossible to follow a physical time transient. Through several computational experiments, the most convenient value of the pseudocompressibility parameter $\beta$ was found to be unity and it is kept constant in the entire domain.

Regarding the momentum equations, the full form

$$\frac{\partial u}{\partial t} + \frac{\partial}{\partial x}\left(u^2 + \frac{p}{\rho} + \tfrac{2}{3}k\right) + \frac{\partial}{\partial y}(uv) + \alpha\frac{uv}{y} = \frac{1}{Re}\left(\frac{\partial \tau_{xx}}{\partial x} + \frac{\partial \tau_{xy}}{\partial y} + \alpha\frac{\tau_{xy}}{y}\right),$$

$$\frac{\partial v}{\partial t} + \frac{\partial}{\partial x}(uv) + \frac{\partial}{\partial y}\left(v^2 + \frac{p}{\rho} + \tfrac{2}{3}k\right) + \alpha\frac{v^2}{y} = \frac{1}{Re}\left(\frac{\partial \tau_{xy}}{\partial x} + \frac{\partial \tau_{yy}}{\partial y} + \alpha\frac{\tau_{yy} - \tau_{\phi\phi}}{y}\right)$$

is used, where $k$ is the kinetic energy, which is taken into account only if a turbulent flow is going to be simulated. Finally, the stresses are

$$\tau_{xx} = 2\nu_{\text{eff}}u_x, \qquad \tau_{yy} = 2\nu_{\text{eff}}v_y, \qquad \tau_{xy} = \nu_{\text{eff}}(u_y + v_x), \qquad \tau_{\varphi\varphi} = 2\nu_{\text{eff}}\frac{v}{y}.$$

### 3.2. *The pressure correction method*

In this method the incompressibility condition is accounted for by the solution of a Poisson equation. Several projection methods have been developed for incompressible flows.[5] The projection method is a fractional step method adapted to the unsteady Navier–Stokes equations. The basic principle of the method is that the evaluation of the time evolution is split into intermediate steps. First a tentative velocity field is calculated by the discretized momentum equations without the pressure gradient. At the second step a Poisson equation is solved and the pressure field is obtained. Finally, the velocity components at the new time level are evaluated by correcting the tentative velocity field using the pressure field.

For the fractional step method described by Anderson and Kristoffersen,[6] the equations used are

$$\frac{u^* - u^n}{\Delta t} + \frac{\partial}{\partial x}(u^2 + \tfrac{2}{3}k) + \frac{\partial}{\partial y}(uv) + \alpha\frac{uv}{y} = \frac{1}{Re}\left(\frac{\partial \tau_{xx}}{\partial x} + \frac{\partial \tau_{xy}}{\partial y} + \alpha\frac{\tau_{xy}}{y}\right),$$

$$\frac{v^* - v^n}{\Delta t} + \frac{\partial}{\partial x}(uv) + \frac{\partial}{\partial y}(v^2 + \tfrac{2}{3}k) + \alpha\frac{v^2}{y} = \frac{1}{Re}\left(\frac{\partial \tau_{xy}}{\partial x} + \frac{\partial \tau_{yy}}{\partial y} + \alpha\frac{\tau_{yy} - \tau_{\phi\phi}}{y}\right),$$

$$\frac{u^{n+1} - u^*}{\Delta t} = \frac{\partial p^{n+1}}{\partial x}, \qquad \frac{v^{n+1} - v^*}{\Delta t} = \frac{\partial p^{n+1}}{\partial y},$$

where $u^*$ and $v^*$ are the components of the tentative velocity. To the first two of the above equations the time-marching scheme of Beam and Warming[1] is applied. The last two equations are combined to give the Poisson equation

$$\frac{\partial^2 p^{n+1}}{\partial x^2} + \frac{\partial^2 p^{n+1}}{\partial y^2} + \alpha \frac{1}{y} \frac{\partial p^{n+1}}{\partial y} = \frac{1}{\Delta t}\left(\frac{\partial u^*}{\partial x} + \frac{\partial v^*}{\partial y} + \alpha \frac{v^*}{y}\right), \tag{2}$$

from which the pressure field is derived.

Finally, the velocity field at the new time level is derived by the relations

$$u^{n+1} = u^* - \Delta t \frac{\partial p^{n+1}}{\partial x}, \qquad v^{n+1} = v^* - \Delta t \frac{\partial p^{n+1}}{\partial y} \tag{3}$$

and mass conservation is satisfied.

### 3.3. *The transformed form of the equations*

A generalized co-ordinate transformation from the physical $(x\ y\ t)$ to the computational $(\xi, \eta, \tau)$ domain is performed. The non-dimensional form of the equations is written as[7]

$$\partial_\tau Q^n + \partial_\xi F^n + \partial_\eta G^n + \alpha E^n = \partial_\xi V^n + \partial_\eta W^n + \alpha C^n + D^n, \tag{4}$$

where $Q$ is the vector of conservative variables, $F$, $G$ and $E$ are the convective fluxes, $V$, $W$ and $C$ are the viscous terms and $D$ is a vector that contains terms of the $k$–$\varepsilon$ equations. These fluxes are different for each of the two methods: for the pseudocompressibility method

$$Q = J^{-1}[p, u, v, k, \varepsilon]^{\mathrm{T}},$$

$$F = J^{-1}\left[\beta U, uU + \xi_x\left(\frac{p}{\rho} + \tfrac{2}{3}k\right), vU + \xi_y\left(\frac{p}{\rho} + \tfrac{2}{3}k\right), kU, \varepsilon U\right]^{\mathrm{T}},$$

$$G = J^{-1}\left[\beta V, uV + \eta_x\left(\frac{p}{\rho} + \tfrac{2}{3}k\right), vV + \eta_y\left(\frac{p}{\rho} + \tfrac{2}{3}k\right), kV, \varepsilon V\right]^{\mathrm{T}},$$

$$E = v(Jy)^{-1}[\beta, u, v, k, \varepsilon]^{\mathrm{T}},$$

$$V = (JRe)^{-1}[0, \xi_x\tau_{xx} + \xi_y\tau_{xy}, \xi_x\tau_{xy} + \xi_y\tau_{yy}, \Gamma_k(\xi_x k_x + \xi_y k_y), \Gamma_\varepsilon(\xi_x\varepsilon_x + \xi_y\varepsilon_y)]^{\mathrm{T}},$$

$$W = (JRe)^{-1}[0, \eta_x\tau_{xx} + \eta_y\tau_{xy}, \eta_x\tau_{xy} + \eta_y\tau_{yy}, \Gamma_k(\eta_x k_x + \eta_y k_y), \Gamma_\varepsilon(\eta_x\varepsilon_x + \eta_y\varepsilon_y)]^{\mathrm{T}},$$

$$C = (JyRe)^{-1}\left[0, \tau_{xy}, \tau_{yy} - \tau_{\phi\phi}, \Gamma_k k_y + 2\nu_t \frac{v^2}{y}, \Gamma_\varepsilon \varepsilon_y + 2\nu_t C_1 \frac{\varepsilon}{k}\frac{v^2}{y}\right]^{\mathrm{T}},$$

$$D = (JRe)^{-1}\left[0, 0, 0, \nu_t G' - Re\ \varepsilon, \nu_t C_1 \frac{\varepsilon}{k} G' - Re\ C_2 \frac{\varepsilon^2}{k}\right]^{\mathrm{T}}$$

and for the pressure correction method

$$Q = J^{-1}[u, v, k, \varepsilon]^{\mathrm{T}},$$

$$F = J^{-1}[uU + \tfrac{2}{3}\xi_x k, vU + \tfrac{2}{3}\xi_y k, kU, \varepsilon U]^{\mathrm{T}},$$

$$G = J^{-1}[uV + \tfrac{2}{3}\eta_x k, vV + \tfrac{2}{3}\eta_y k, kV, \varepsilon V]^{\mathrm{T}},$$

$$E = v(Jy)^{-1}[u, v, k, \varepsilon]^{\mathrm{T}},$$

$$V = (JRe)^{-1}[\xi_x\tau_{xx} + \xi_y\tau_{xy},\ \xi_x\tau_{xy} + \xi_y\tau_{yy},\ \Gamma_k(\xi_x k_x + \xi_y k_y),\ \Gamma_\varepsilon(\xi_x\varepsilon_x + \xi_y\varepsilon_y)]^T,$$

$$W = (JRe)^{-1}[\eta_x\tau_{xx} + \eta_y\tau_{xy},\ \eta_x\tau_{xy} + \eta_y\tau_{yy},\ \Gamma_k(\eta_x k_x + \eta_y k_y),\ \Gamma_\varepsilon(\eta_x\varepsilon_x + \eta_y\varepsilon_y)]^T,$$

$$C = (JyRe)^{-1}\left[\tau_{xy},\ \tau_{yy} - \tau_{\phi\phi},\ \Gamma_k k_y + 2\nu_t\frac{v^2}{y},\ \Gamma_\varepsilon\varepsilon_y + 2\nu_t C_1\frac{\varepsilon}{k}\frac{v^2}{y}\right]^T,$$

$$D = (JRe)^{-1}\left[0,\ 0,\ \nu_t G' - Re\ \varepsilon,\ \nu_t C_1\frac{\varepsilon}{k}G' - Re\ C_2\frac{\varepsilon^2}{k}\right]^T.$$

As can be seen, the flux $C$ contains in addition the axisymmetric terms of the production term $\tilde{G}$, which now takes the form

$$G' = [2(\xi_x u_\xi + \eta_x u_\eta)^2 + 2(\xi_y v_\xi + \eta_y v_\eta)^2 + (\xi_x v_\xi + \eta_x v_\eta + \xi_y u_\xi + \eta_y u_\eta)^2].$$

In the expressions above $\xi$ and $\eta$ are the curvilinear co-ordinates connected to the Cartesian co-ordinates $x$ and $y$ through the generalized co-ordinate transformation

$$\xi = \xi(x, y, t), \qquad \eta = \eta(x, y, t), \qquad \tau = t,$$

and

$$J = \xi_x\eta_y - \xi_y\eta_x$$

is the Jacobian of the transformation. Finally, $U$ and $V$are the contravariant velocities along the directions $\xi$ and $\eta$ respectively, given by the relations

$$U = \xi_t + \xi_x u + \xi_y v, \qquad V = \eta_t + \eta_x u + \eta_y v.$$

## 4. NUMERICAL ALGORITHM AND METHOD OF APPLICATION

### *4.1. The time-marching scheme*

For the solution of the system of equation (4) the implicit, factored, finite difference scheme of Beam and Warming[1] is used. The temporal derivative in (4) is approximated via a generalized time differencing as

$$\Delta Q^n = \frac{\theta\Delta\tau}{1+\zeta}\partial_\tau\Delta Q^n + \frac{\Delta\tau}{1+\zeta}\partial_\tau Q^n + \frac{\zeta}{1+\zeta}\Delta Q^{n-1} + O[(\theta - \tfrac{1}{2} - \zeta)\Delta\tau^2 + \Delta\tau^3], \tag{5}$$

where $\Delta Q^n = Q^{n+1} - Q^n$ for the artificial compressibility method and $\Delta Q^n = Q^* - Q^n$ for the pressure correction method. According to the choice of the values of $\theta$ and $\zeta$ in (5), a first- or second-order time-accurate scheme can be derived. In the present study, setting $\theta = 1$ and $\zeta = 0$, the first-order Euler implicit scheme is used and first-order time accuracy is obtained.

After substituting (4) into (5) and performing calculations, a non-linear expression results for the time increment of the vector of conservatives variables, $\Delta Q^n$. In order to derive a linear algebraic system of equations, a linearization of viscous and inviscid fluxes must be performed. The inviscid fluxes, which are functions of $Q$, are linearized using Taylor series expansion as

$$\Delta F^n = A^n\Delta Q^n + O(\Delta\tau^2), \qquad \Delta G^n = B^n\Delta Q^n + O(\Delta\tau^2),$$

where $A^n = \partial F^n/\partial Q^n$ and $B^n = \partial G^n/\partial Q^n$ are the Jacobian matrices of the vectors $F^n$ and $G^n$ respectively: for the pseudocompressibility method

$$A^n,\ B^n = \begin{vmatrix} 0 & \beta\alpha_x & \beta\alpha_y & 0 & 0 \\ \alpha_x & \alpha_t + 2\alpha_x u + \alpha_y v & \alpha_y u & \tfrac{2}{3}\alpha_x & 0 \\ \alpha_y & \alpha_x v & \alpha_t + \alpha_x u + 2\alpha_y v & \tfrac{2}{3}\alpha_y & 0 \\ 0 & k\alpha_x & k\alpha_y & \alpha_t + \alpha_x u + \alpha_y v & 0 \\ 0 & \varepsilon\alpha_x & \varepsilon\alpha_y & 0 & \alpha_t + \alpha_x u + \alpha_y v \end{vmatrix}$$

and for the pressure correction method

$$A^n,\ B^n = \begin{vmatrix} \alpha_t + 2\alpha_x u + \alpha_y v & \alpha_y u & \tfrac{2}{3}\alpha_x & 0 \\ \alpha_x v & \alpha_t + \alpha_x u + 2\alpha_y v & \tfrac{2}{3}\alpha_y & 0 \\ k\alpha_x & k\alpha_y & \alpha_t + \alpha_x u + \alpha_y v & 0 \\ \varepsilon\alpha_x & \varepsilon\alpha_y & 0 & \alpha_t + \alpha_x u + \alpha_y v \end{vmatrix},$$

where $\alpha = \xi$ for $A^n$ and $\alpha = \eta$ for $B^n$.

The above linearization of the inviscid fluxes ensures the second-order time accuracy of the scheme. In order that this accuracy is retained in the corresponding linearization of the viscous fluxes, it must be taken into account that the latter are functions of all $Q$, $Q_\xi$ and $Q_\eta$. Then the viscous fluxes $V^n$, $W^n$ and $C^n$ are first split into two parts, one of which is a function of $Q$ and $Q_\xi$ and the other a function of $Q$ and $Q_\eta$:

$$V^n(Q, Q_\xi, Q_\eta) = V_1^n(Q, Q_\xi) + V_2^n(Q, Q_\eta), \qquad W^n(Q, Q_\xi, Q_\eta) = W_1^n(Q, Q_\xi) + W_2^n(Q, Q_\eta),$$

$$C^n(Q, Q_\xi, Q_\eta) = C_1^n(Q, Q_\xi) + C_2^n(Q, Q_\eta) + C_3^n,$$

where

$$C_3^n = v(JRe\ y^2)^{-1}\left[0, 0, -2v_{\text{eff}}, 2v_t v, 2v_t C_1 \frac{\varepsilon}{k} v\right]^T.$$

The vectors $V_1^n$ and $W_2^n$ are linearized implicitly using Taylor series expansion as

$$\Delta V_1^n = (P^n - R_\xi^n)\Delta Q^n + \partial_\xi(R\Delta Q)^n + O(\Delta\tau^2),$$

$$\Delta W_2^n = (Y^n - S_n^n)\Delta Q^n + \partial_\eta(S\Delta Q)^n + O(\Delta\tau^2),$$

while the vectors $V_2^n$ and $W_1^n$ are linearized explicitly as

$$\Delta V_2^n = \Delta V_2^{n-1} + O(\Delta\tau^2), \qquad \Delta W_1^n = \Delta W_1^{n-1} + O(\Delta\tau^2).$$

The Jacobian matrices for the pseudocompressibility method are

$$R^n,\ S^n = \frac{1}{Re}\begin{vmatrix} 0 & 0 & 0 & 0 & 0 \\ 0 & v_{\text{eff}}(2\alpha_x^2 + \alpha_y^2) & v_{\text{eff}}\alpha_x\alpha_y & 0 & 0 \\ 0 & v_{\text{eff}}\alpha_x\alpha_y & v_{\text{eff}}(\alpha_x^2 + 2\alpha_y^2) & 0 & 0 \\ 0 & 0 & 0 & \Gamma_k(\alpha_x^2 + \alpha_y^2) & 0 \\ 0 & 0 & 0 & 0 & \Gamma_\varepsilon(\alpha_x^2 + \alpha_y^2) \end{vmatrix},$$

$(-P + R_\xi)^n$, $(-Y + S_\eta)^n$

$$= \frac{J}{Re}\begin{vmatrix} 0 & 0 & 0 & 0 & 0 \\ 0 & \partial_\alpha\left(\frac{\nu_{\text{eff}}(2\alpha_x^2+\alpha_y^2)}{J}\right) & \partial_\alpha\left(\frac{\nu_{\text{eff}}\alpha_x\alpha_y}{J}\right) & 0 & 0 \\ 0 & \partial_\alpha\left(\frac{\nu_{\text{eff}}\alpha_x\alpha_y}{J}\right) & \partial_\alpha\left(\frac{\nu_{\text{eff}}(\alpha_x^2+2\alpha_y^2)}{J}\right) & 0 & 0 \\ 0 & 0 & 0 & \partial_\alpha\left(\frac{\Gamma_k(\alpha_x^2+\alpha_y^2)}{J}\right) & 0 \\ 0 & 0 & 0 & 0 & \partial_\alpha\left(\frac{\Gamma_\varepsilon(\alpha_x^2+\alpha_y^2)}{J}\right) \end{vmatrix},$$

where $\alpha = \xi$ for $R^n$ and $(-P + R_\xi)^n$ and $\alpha = \eta$ for $S^n$ and $(-Y + S_\eta)^n$.

The fluxes $C_1^n$, $C_2^n$, and $C_3^n$ are linearized in the same way as the inviscid fluxes and the Jacobian matrices $N_1^n = \partial C_1^n/\partial Q^n$, $N_2^n = \partial C_2^n/\partial Q^n$ and $N_3^n = \partial C_3^n/\partial Q^n$ for the artificial compressibility method are

$$N_1^n, N_2^n = \frac{J_\alpha}{JRe\,y}\begin{vmatrix} 0 & 0 & 0 & 0 & 0 \\ 0 & \nu_{\text{eff}}\alpha_y & \nu_{\text{eff}}\alpha_x & 0 & 0 \\ 0 & 0 & 2\nu_{\text{eff}}\alpha_y & 0 & 0 \\ 0 & 0 & 0 & \alpha_y\Gamma_k & 0 \\ 0 & 0 & 0 & 0 & \alpha_y\Gamma_\varepsilon \end{vmatrix},$$

$$N_3^n = \frac{2}{y^2}\begin{vmatrix} 0 & 0 & 0 & 0 & 0 \\ 0 & 0 & 0 & 0 & 0 \\ 0 & 0 & -\frac{\nu_{\text{eff}}}{Re} & 0 & 0 \\ 0 & 0 & 0 & 2C_\mu v^2\frac{k}{\varepsilon} & -C_\mu v^2\frac{k^2}{\varepsilon^2} \\ 0 & 0 & 0 & C_\mu C_1 v^2 & 0 \end{vmatrix},$$

where $\alpha = \xi$ for $N_1^n$ and $\alpha = \eta$ for $N_2^n$.

The same linearization is used for the fluxes $E^n$ and $D^n$ and the Jacobian matrices $T^n = \partial E^n/\partial Q^n$ and $H^n = \partial D^n/\partial Q^n$ obtained for the artificial compressibility method are

$$T^n = \frac{1}{y}\begin{vmatrix} 0 & 0 & 1 & 0 & 0 \\ 0 & v & u & 0 & 0 \\ 0 & 0 & 2v & 0 & 0 \\ 0 & 0 & k & v & 0 \\ 0 & 0 & \varepsilon & 0 & v \end{vmatrix}, \qquad H^n = \begin{vmatrix} 0 & 0 & 0 & 0 & 0 \\ 0 & 0 & 0 & 0 & 0 \\ 0 & 0 & 0 & 0 & 0 \\ 0 & 0 & 0 & 2C_\mu\frac{k}{\varepsilon}G' & -C_\mu\frac{k^2}{\varepsilon^2}G' - 1 \\ 0 & 0 & 0 & C_\mu C_1 G' + C_2\frac{\varepsilon^2}{k^2} & -2C_2\frac{\varepsilon}{k} \end{vmatrix},$$

where the production term $G'$ is considered to be constant. For the pressure correction method the Jacobian matrices are derived from the corresponding matrices of the pseudocompressibility method by deleting the first line and the first column.

Substitution of the linear expressions for the flux vectors into the original non-linear equation for $\Delta Q^n$ leads to a strongly coupled system of equations in both spatial directions. This coupled system is solved by the approximate factorization technique[1] in two sweeps, $\xi$ and $\eta$, which in the present case are

$$\left(I + \frac{\theta\Delta\tau}{1+\zeta}\left[\partial_\xi(A - P + R_\xi) - \partial_{\xi\xi}R - \alpha N_1 + \Theta_a H\right]^n\right)\cdot \Delta\tilde{Q}^n = \mathrm{RHS}, \tag{6a}$$

$$\left(I + \frac{\theta\Delta\tau}{1+\zeta}\left[\partial_\eta(B - Y + S_\eta) - \partial_{\eta\eta}S - \alpha(N_2 + N_3 - T) + \Theta_b H\right]^n\right)\cdot \Delta Q^n = \Delta\tilde{Q}^n, \tag{6b}$$

where

$$\bar{Q}^{n+1} = \bar{Q}^n + J\Delta Q^n \quad \text{or} \quad \bar{Q}^* = \bar{Q}^n + J\Delta Q^n \tag{6c}$$

for the pseudocompressibility or the pressure correction method respectively,

$$\mathrm{RHS} = \frac{\Delta\tau}{1+\zeta}\left[\partial_\xi(-F + V)^n + \partial_\eta(-G + W)^n + \alpha(C - E)^n + D^n\right] + \frac{\theta\Delta\tau}{1+\zeta}(\partial_\xi\Delta V_2^{n-1} + \partial_\eta\Delta W_1^{n-1})$$
$$+ \frac{\zeta}{1+\zeta}\Delta U^{n-1} + D_e + O[(\theta - \tfrac{1}{2} - \zeta)\Delta\tau^2 + \Delta\tau^3], \tag{7}$$

$\bar{Q} = JQ$ is the vector of conservative variables in the physical domain, $D_e$ represents the artificial dissipation terms and $\Theta_a$ and $\Theta_b$ are weighting functions[8] used to add the Jacobian matrix $H$ in both sweeps. Although in the present study this was found to have no effect on the final results, these expressions allow us to introduce $H$ in the sweep where the largest gradients occur and are given by the relations

$$\Theta_a = \frac{|V|}{(U^2 + V^2)^{1/2}}, \qquad \Theta_b = \frac{|U|}{(U^2 + V^2)^{1/2}}.$$

It should be noticed that when the pseudocompressibility method is used, equation (6c) provides the conservative values of the physical field. In contrast, when the pressure correction method is used, this equation provides the values of the tentative field and equations (2) and (3) must be used to provide the physical field.

### *4.2. The artificial compressibility terms*

The spatial derivatives in the above system of equations are approximated by central second-order derivatives. Thus the solution of the system of equations (6) requires the inversion of two block-tridiagonal systems, one in each direction. On the other hand, the use of central differences leads to the necessity of adding external artificial dissipation terms, so that the stability is retained and oscillations from the solution are removed. In the present work only explicit terms $D_e$ are used in (7).

The following fourth-order dissipation terms were used initially,

$$D_e = -\Omega_e\Delta\tau J^{-1}[(\Delta_\xi\nabla_\xi)^2(JQ) + (\Delta_\eta\nabla_\eta)^2(JQ)],$$

where $\Omega_e$ is a user-defined constant. It was found that these terms were insufficient to handle the $k$–$\varepsilon$ equations properly and to remove the negative values that occurred near the solid boundaries. Thus the blended second- and fourth-order non-linear model, first introduced by Jameson *et al.*[9] and slightly altered by Pulliam[10] and other researchers,[11] was used for the first time in incompressible flows:

$$D_e = \nabla_\xi[\sigma^{(\xi)}_{i,j}(e^{(\xi)(2)}_{i,j}\Delta_\xi JQ - e^{(\xi)(4)}_{i,j}\Delta_\xi\nabla_\xi\Delta_\xi JQ)] + \nabla_\eta[\sigma^{(\eta)}_{i,j}(e^{(\eta)(2)}_{i,j}\Delta_\eta JQ - e^{(\eta)(4)}_{i,j}\Delta_\eta\nabla_\eta\Delta_\eta JQ)].$$

In the expression above $\nabla_\xi$, $\nabla_\eta$ and $\Delta_\xi$, $\Delta_\eta$ are the backward and forward difference operators respectively given by the relations

$$\Delta_\xi a_{i,j} = a_{i+1,j} - a_{i,j}, \qquad \nabla_\xi a_{i,j} = a_{i,j} - a_{i-1,j},$$

with corresponding expressions for the $\eta$-direction, and $\sigma^{(\xi)}$ and $\sigma^{(\eta)}$ are non-linear scaling coefficients intended to scale all the dissipation terms by the local eigenvalues of the solution. Two types of these coefficients were used,

$$\sigma^{(\xi)}_{i,j} = J^{-1}_{i,j}(\lambda^\xi_{i,j} + \lambda^\eta_{i,j}) + J^{-1}_{i+1,j}(\lambda^\xi_{i+1,j} + \lambda^\eta_{i+1,j}), \qquad \sigma^{(\eta)}_{i,j} = J^{-1}_{i,j}(\lambda^\xi_{i,j} + \lambda^\eta_{i,j}) + J^{-1}_{i,j+1}(\lambda^\xi_{i,j+1} + \lambda^\eta_{i,j+1})$$

and

$$\sigma^{(\xi)}_{i,j} = J^{-1}_{i,j}\lambda^\xi_{i,j} + J^{-1}_{i+1,j}\lambda^\xi_{i+1,j}, \qquad \sigma^{(\eta)}_{i,j} = J^{-1}_{i,j}\lambda^\eta_{i,j} + J^{-1}_{i,j+1}\lambda^\eta_{i,j+1},$$

but no significant differences occurred. In the equations above $\lambda^\xi$ and $\lambda^\eta$ are the largest eigenvalues of the Jacobian matrices $A$ and $B$ respectively.

For the pseudocompressibility method the eigenvalues are

$$\lambda^\xi_{i,j} = |U|_{i,j} + \sqrt{[U^2 + \beta(\xi_x^2 + \xi_y^2)]}|_{i,j}, \qquad \lambda^\eta_{i,j} = |V|_{i,j} + \sqrt{[V^2 + \beta(\eta_x^2 + \eta_y^2)]}|_{i,j} \tag{8a}$$

and for the pressure correction method

$$\lambda^\xi_{i,j} = 3|U|_{i,j}, \qquad \lambda^\eta_{i,j} = 3|V|_{i,j}. \tag{8b}$$

The coefficients $e^{(2)}$ and $e^{(4)}$ are used to switch from fourth- to second-order damping in regions with large pressure gradients, avoiding the appearance of oscillations, or large dissipation gradients, avoiding the appearance of negative $k$–$\varepsilon$ values:

$$e^{(\xi)(2)}_{i,j} = k_2\Delta\tau\ \max(\nu^\xi_{i+1,j}, \nu^\xi_{i,j}, \nu^\xi_{i-1,j}), \qquad e^{(\eta)(2)}_{i,j} = k_2\Delta\tau\ \max(\nu^\eta_{i,j+1}, \nu^\eta_{i,j}, \nu^\eta_{i,j-1}),$$

$$e^{(\xi)(4)}_{i,j} = \max(0,\ k_4\Delta\tau - e^{(\xi)(2)}_{i,j}), \qquad e^{(\eta)(4)}_{i,j} = \max(0,\ k_4\Delta\tau - e^{(\eta)(2)}_{i,j}),$$

where $k_2$ and $k_4$ are constants and $\nu$ is a dissipation sensor used to identify the presence of large pressure gradients for the momentum equations,

$$\nu^\xi_{i,j} = \left|\frac{p_{i+1,j} - 2p_{i,j} + p_{i-1,j}}{p_{i+1,j} + 2p_{i,j} + p_{i-1,j}}\right|, \qquad \nu^\eta_{i,j} = \left|\frac{p_{i,j+1} - 2p_{i,j} + p_{i,j-1}}{p_{i,j+1} + 2p_{i,j} + p_{i,j-1}}\right|,$$

or large dissipation gradients[12] for the $k$–$\varepsilon$ equations,

$$\nu^\xi_{i,j} = \left|\frac{\varepsilon_{i+1,j} - 2\varepsilon_{i,j} + \varepsilon_{i-1,j}}{\varepsilon_{i+1,j} + 2\varepsilon_{i,j} + \varepsilon_{i-1,j}}\right|, \qquad \nu^\eta_{i,j} = \left|\frac{\varepsilon_{i,j+1} - 2\varepsilon_{i,j} + \varepsilon_{i,j-1}}{\varepsilon_{i,j+1} + 2\varepsilon_{i,j} + \varepsilon_{i,j-1}}\right|.$$

The constants that appear in the expressions above are held at the constant values

$$k_2 = 0{\cdot}25, \qquad k_4 = 0{\cdot}01.$$

Via numerical experiments it was found that the best results were obtained with the following values of the constants for the $k$–$\varepsilon$ equations:

$$k_2 = 0{\cdot}15, \qquad k_4 = 0{\cdot}01.$$

It should be mentioned that in the pressure correction method no artificial dissipation terms are used for the solution of the Poisson equation.

### 4.3. *The solution of the Poisson equation*

According to the coordinate transformation described above, the Poisson equation (2) takes the conservative form

$$\partial_\xi(Ap_\xi + Bp_\eta) + \partial_\eta(Bp_\xi + Cp_\eta) = D, \tag{9}$$

where

$$A = J(x_\eta^2 + y_\eta^2), \qquad B = J(-x_\xi x_\eta - y_\xi y_\eta), \qquad C = J(x_\xi^2 + y_\xi^2),$$

$$D = \frac{1}{\Delta\tau}\left((u^* y_\eta)_\xi + (-u^* y_\xi)_\eta + (-v^* x_\eta)_\xi + (v^* x_\xi)_\eta + \alpha\frac{v^*}{y}\right) + \frac{a}{y}[(p^{n+1}x_\eta)_\xi + (-p^{n+1}x_\xi)_\eta].$$

Applying the explicit iterative method to solve (9), we obtain

$$p_{i,j}^{k+1} = \left(\frac{A_\xi + B_\eta}{2}(p_{i+1,j}^k - p_{i-1,j}^k) + \frac{B_\xi + C_\eta}{2}(p_{i,j+1}^k - p_{i,j-1}^k) + A(p_{i+1,j}^k + p_{i-1,j}^k)\right.$$
$$\left. + C(p_{i,j+1}^k + p_{i,j-1}^k) + \tfrac{1}{2}B(p_{i+1,j+1}^k - p_{i-1,j+1}^k - p_{i+1,j-1}^k + p_{i-1,j-1}^k) - D^k\right)\Big/(2A + 2C),$$

where the superscript $k$ denotes the index of internal iteration.

It was found that this method is much faster than the classical point Gauss–Seidel technique. At each time step 100 Poisson equation iterations are done unless a specified convergence criterion is reached. After several time steps this criterion is reached in a few iterations and mass conservation is satisfied. The boundary conditions for the pressure are applied at each internal iteration, while the tentative velocity field remains constant in the entire domain.

### 4.4. *The definition of the time step*

Although the solution method is implicit, the actual stability of the scheme is not independent of the time step used. The time step in the present work is computed by the well-known local time-stepping technique for steady state problems, which takes into account the variation in the flow in combination with the variation in the grid spacing:

$$\Delta\tau|_{i,j} = \frac{\Delta\tau_{\text{ref}}}{\lambda_{i,j}^\xi + \lambda_{i,j}^\eta},$$

where $\Delta\tau_{\text{ref}}$ is the initially user-defined reference time step, which for the present work is equal to unity, and $\lambda^\xi$ and $\lambda^\eta$ are given by (8a) or (8b) depending on which method is used.

## 5. BOUNDARY CONDITIONS

Throughout the computations, explicit boundary conditions are used. On the inlet boundary the velocity profiles are specified, the pressure second derivative is set equal to zero and the kinetic energy $k_{in}$ and dissipation $\varepsilon_{in}$ are given by the empirical relations

$$k_{in} = 0{\cdot}003u_{ref}^2, \qquad \varepsilon_{in} = \frac{C_\mu k_{in}^{1{\cdot}5}}{0{\cdot}03D_{in}},$$

where $u_{ref}$ is the reference velocity and $D_{in}$ is the inlet diameter.

On the outlet boundary all variables are calculated by extrapolation from the interior, while the pressure is set to its reference value. At the symmetry axis the first derivatives of all variables are set equal to zero, except the $v$-component of the velocity which is set equal to zero. On the far-field boundary of the aerofoil case the velocities are specified by the relations $u_{in} = u_{ref} \cos \alpha$ and $v_{in} = u_{ref} \sin \alpha$, where $\alpha$ is the angle of attack, and the pressure first derivative is set equal to zero. On the outflow boundary first derivatives equal to zero are applied to all variables, except to the pressure which takes its reference value. On the wake cut points the conservative variables are defined by averaging their values from both sides of the wake.

On the solid surface the non-slip condition is applied for the velocity components. The kinetic energy and dissipation are defined at the first grid point above the solid surface by use of the wall functions (1). The pressure is derived from the assumption of a zero normal pressure gradient, which is obtained by the momentum equations and demands the solution of a tridiagonal system at each time step.

## 6. RESULTS AND VALIDATION

### 6.1. *Laminar flow over a backward-facing step*

The steady, viscous, incompressible, isothermal, laminar flow over a two-dimensional backward-facing step is the first test case selected to test our algorithm. The test case characteristics are given by Gartling.[13] The downstream part of the channel was defined to have unit height $H$, with the step height and the upstream inlet region both set equal to $H/2$. The downstream channel length was taken to be $L = 30H$, i.e. the channel extends 60 step heights from the inlet (Figure 1). Two grids, 99 × 41 and 155 × 51, were used to simulate

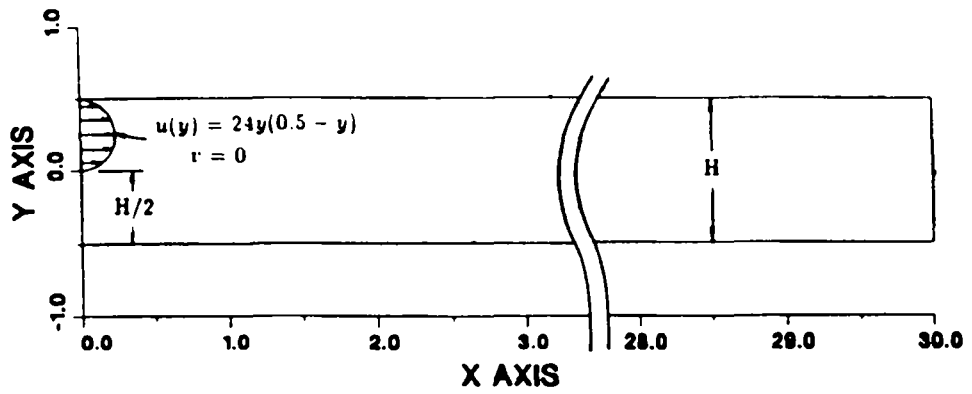


Figure 1. Backward-facing step geometry with channel dimensions—$Re = 800$

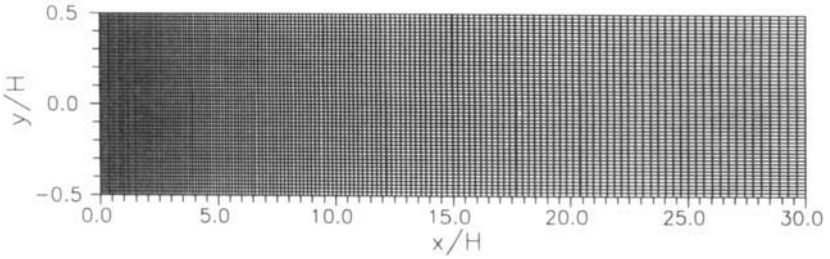


Figure 2. General view of 155 × 51 grid—$Re$ = 800

the flow. In Figure 2 the denser grid is shown. Each of the two methods was tested on both grids.

The boundary conditions applied are those described in the previous section. The inlet velocity field was specified as a parallel flow with a parabolic horizontal component[13] given by $u(y) = 24y(0{\cdot}5 - y)$ for $0 \leqslant y \leq 0{\cdot}5$ (Figure 1). This produces a maximum velocity $u_{max} = 1{\cdot}5$ and an average inflow reference velocity $u_{ref} = 1{\cdot}0$. After a solution had been obtained, the pressure field was adjusted such that the pressure level was zero at the step corner ($x = 0$, $y = 0$). The Reynolds number is defined by $Re = u_{ref}H/\nu$ and for the present case is equal to 800.

In Figure 3 the streamfunction contours are presented, which were found to be almost identical for all combinations of methods and grids. This figure shows that two recirculation regions exist, one on the lower wall and another on the upper wall.

In Figures 4 and 5 the pressure profiles along the lower and upper walls respectively are presented. In Figure 6 the pressure profiles at $x/H = 7$ and 15 are shown. The conclusion is that both methods are in good agreement with Gartling's results, with the pressure correction method having a slight superiority. The same conclusion is deduced from Figures 7 and 8, where the velocity profiles at $x/H = 7$ and 15 are presented.

In Table I the recirculation regions yielded by the current methods are compared with those given by Gartling. As can be seen, the predicted separation and reattachment points are in very good agreement with the numerical results of Gartling. It should be mentioned that the pressure correction method gives results that are closer to the other numerical results in comparison with those obtained from the pseudocompressibility method. In addition, grid refinement plays a dominant role in the prediction of the recirculation zones, although it has negligible influence on the pressure and velocity profiles. On the other hand, it is clear that the results are not affected when fourth-order dissipation terms are used instead of blended second- and fourth-order dissipation terms.

In the same table it is seen that the pressure correction method needs many more iterations to converge than the pseudocompressibility method. One reason for this is that the Poisson

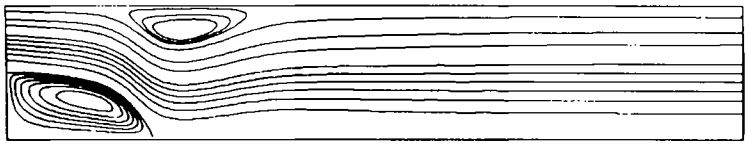

Figure 3. Streamfunction contours for 155 × 51 grid; the level values are[9] −0·030, −0·025, −0·020, −0·015, −0·010, −0·005, 0·000, 0·050, 0·100, 0·150, 0·200, 0·250, 0·300, 0·350, 0·400, 0·450, 0·490, 0·500, 0·502, 0·504—$Re$- = 800

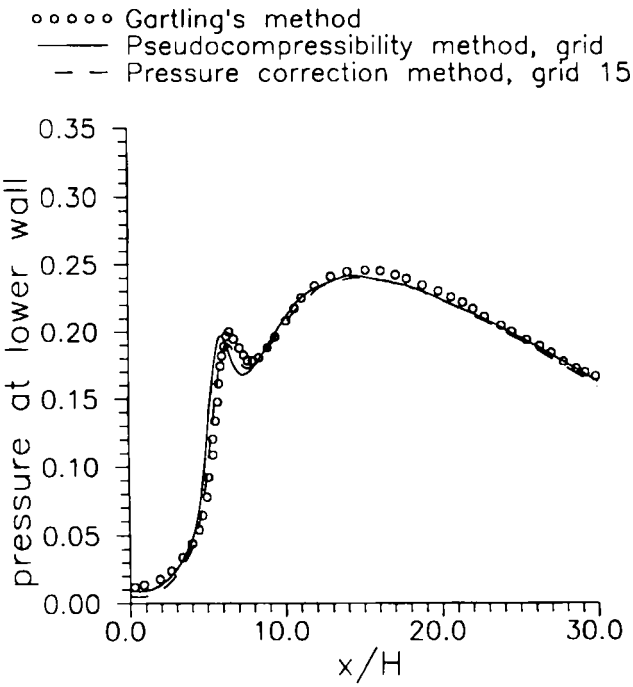


Figure 4. Pressure profiles along lower wall backward-facing step, $Re = 800$

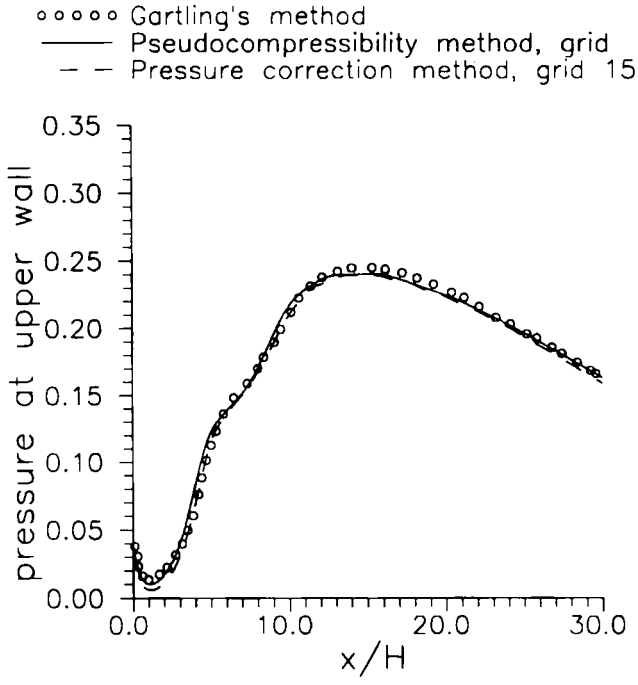


Figure 5. Pressure profiles along upper wall—backward-facing step, $Re = 800$

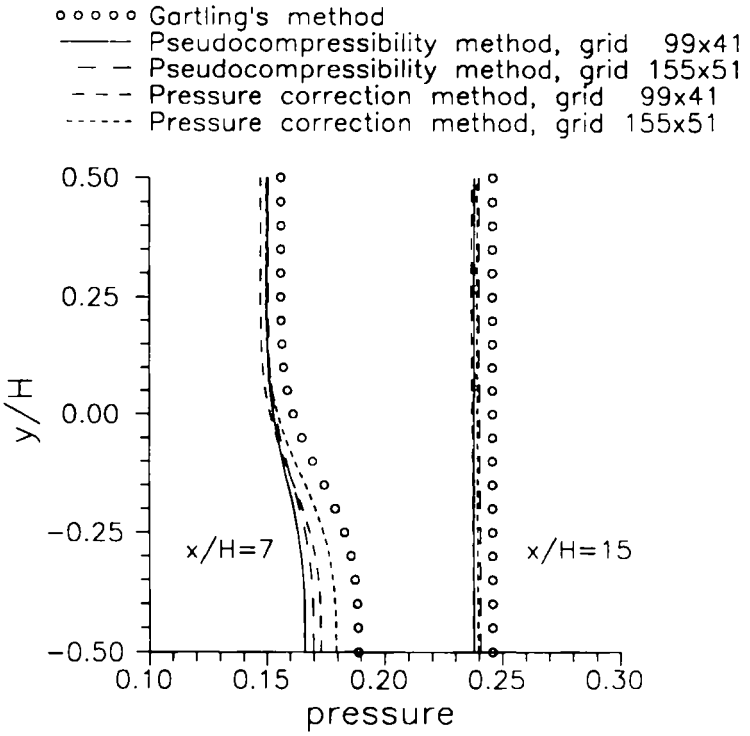


Figure 6. Pressure profiles across channel at $x/H = 7$ and 15—backward-facing step, $Re = 800$

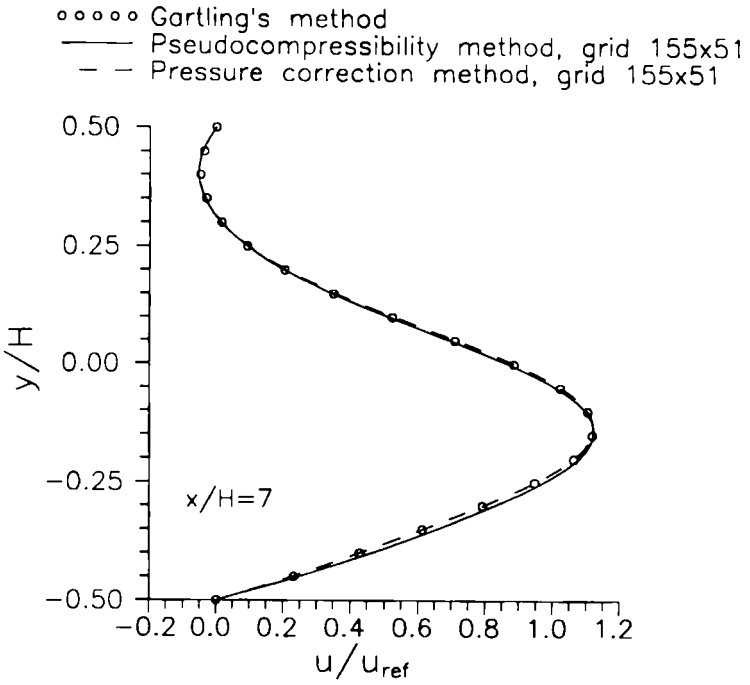


Figure 7. Velocity profiles at $x/H = 7$—backward-facing step, $Re = 800$

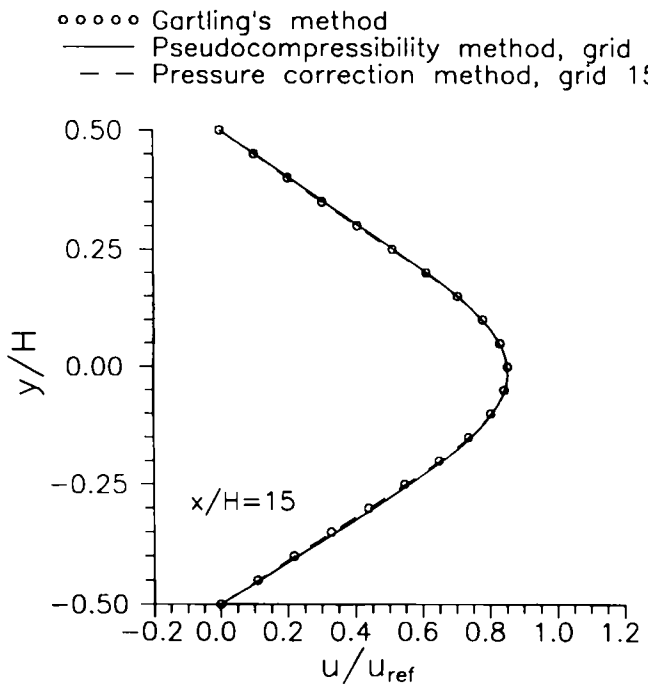


Figure 8. Velocity profiles at $x/H = 15$ - backward-facing step, $Re = 800$

equation is solved without the use of any artificial dissipation terms. In Figure 9 the convergence history is shown for all the conservative variables.

### 6.2. *Turbulent flow over an NACA 0012 aerofoil*

The first turbulent case under consideration is the external flow over an NACA 0012 aerofoil.[14] The Reynolds number, based on the chord length $c$ and freestream velocity $u_{inf}$, is $2{\cdot}8 \times 10^6$ and the angle of attack is $\alpha = 0°$.

Three grids, $99 \times 77$, $157 \times 77$ and $89 \times 51$, were used for the current case. The numbers of points distributed on the aerofoil surface are 67, 107 and 59 and in the wake 16, 25 and 15 respectively. The front boundary was placed 11 chords in front of the aerofoil, the top and bottom boundaries 12 chords away and the rear boundary 8 chords behind. in Figure 10 the $99 \times 77$ grid is shown.

In Figure 11 the surface pressure distribution is plotted and compared with the experimental data of Gregory and O'Reilly[15] and the computational results of Shamroth and Gibeling.[16] The results obtained by the two methods are better than the other computational results. In addition, the pressure correction method shows better behaviour at the trailing edge than the pseudocompressibility method.

### 6.3. *Turbulent flow over a 45° axisymmetric diffuser*

The turbulent flow in a 45° axisymmetric diffuser is investigated. The Reynolds number, based on the inlet section height $H$ and mean velocity $u_{ref}$, is $2 \times 10^5$. The step's origin is at

Table I. Comparison of predicted recirculation regions and numbers of iterations to achieve convergence for laminar flow over a backward-facing step

| Method | Grid | Lower wall | | Upper wall | | Convergence |
|---|---|---|---|---|---|---|
| | | Separation $x/H$ | Reattachment $x/H$ | Separation $x/H$ | Reattachment $x/H$ | No. of iterations to $1 \times 10^{-4}$ |
| Gartling[13] | 800 × 40 | 0·00 | 6·10 | 4·79 | 10·48 | |
| Pseudocompressibility | 99 × 41 | 0·00 | 5·44 | 4·60 | 9·54 | 4949 |
| Pressure correction | 99 × 41 | 0·00 | 5·75 | 4·60 | 10·09 | 7072 |
| Pseudocompressibility | 155 × 51 | 0·00 | 5·51 | 4·65 | 9·74 | 6287 |
| Pressure correction | 155 × 51 | 0·00 | 5·93 | 4·78 | 10·21 | 10777 |
| Pseudocompressibility with 4th order dissipation | 99 × 41 | 0·00 | 5·46 | 4·60 | 9·55 | 4942 |

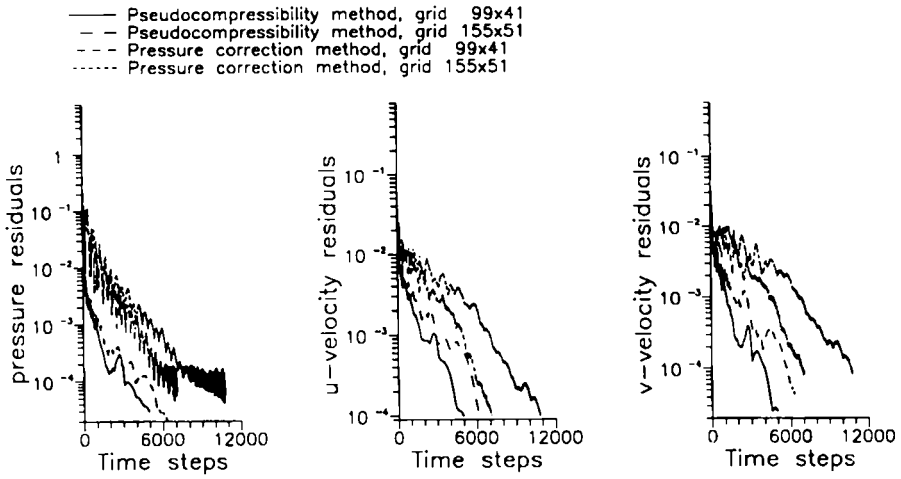


Figure 9. Convergence histories for all conservative variables backward-facing step, $Re = 800$

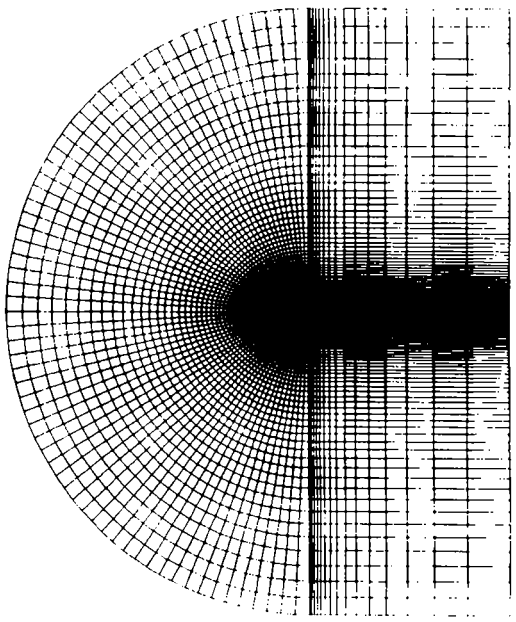

Figure 10. General view of 99 × 77 grid used for NACA 0012 aerofoil test case $-Re = 2{\cdot}8 \times 10^6$, $\alpha = 0°$

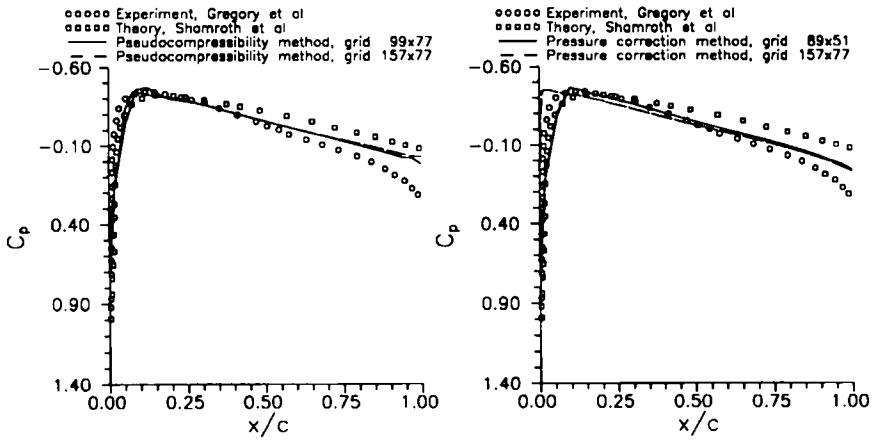


Figure 11. Surface pressure distributions for NACA 0012 aerofoil—$Re = 2{\cdot}8 \times 10^6$, $\alpha = 0^\circ$

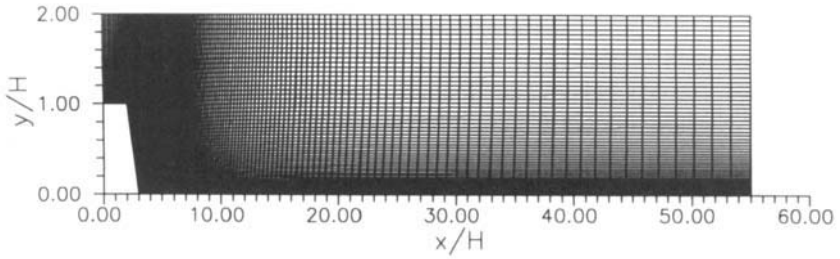


Figure 12. General view of 155 × 55 grid used for 45° axisymmetric diffuser

$x/H = 2$ and its end at $x/H = 3$. The upper boundary is a symmetry axis. Two grids, 99 × 37 and 155 × 55, were used. The exit is located 40 step heights from the inlet for the coarse grid and 55 step heights from the inlet for the dense grid. In Figure 12 the 155 × 55 grid is presented.

In Table II the recirculation regions provided by the two methods are presented and compared with the experimental data of Chaturvedi[17] and other numerical results of Michelassi and

Table II. Comparison of predicted recirculation lengths for turbulent flow over a 45° axisymmetric diffuser

| Method | Grid | Separation $x/H$ | Reattachment $x/H$ | Recirculation length |
|---|---|---|---|---|
| Experiment[17] | | | | 9·00$H$ |
| Pseudocompressibility | 99 × 37 | 2·05 | 11·41 | 9·36$H$ |
| Pressure correction | 99 × 37 | 2·06 | 11·84 | 9·78$H$ |
| Pseudocompressibility | 155 × 55 | 2·04 | 12·67 | 10·63$H$ |
| Pressure correction | 155 × 55 | 2·04 | 12·27 | 10·23$H$ |
| Michelassi and Benocci[8] (CH) | 80 × 45 | | (2D) | 7·75$H$ |
| Michelassi and Benocci[8] (TL) | 80 × 45 | | (2D) | 8·40$H$ |

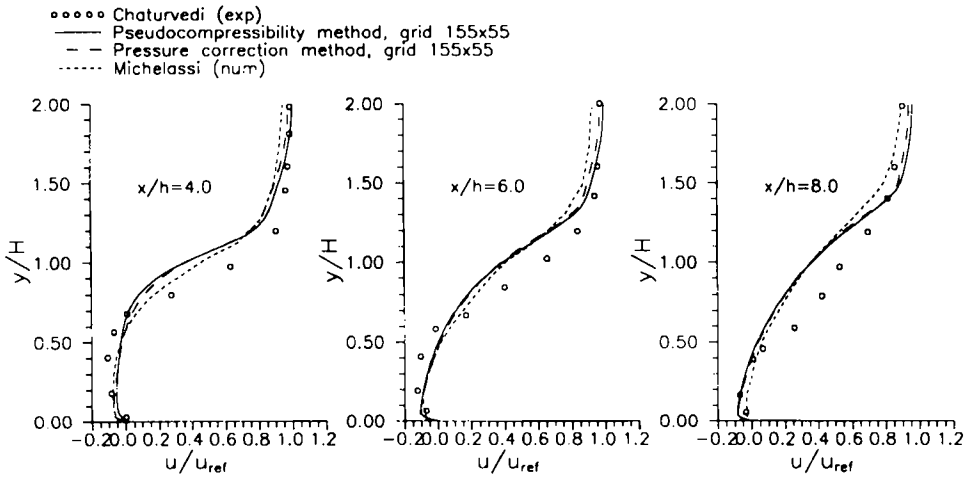


Figure 13. Mean velocity profiles for 45° axisymmetric diffuser $Re = 2 \times 10^5$

Benocci.[8] As can be seen in this table, both methods overestimate the recirculation zone. It should be mentioned that Michelassi and Benocci considered the diffuser to be two-dimensional and used the low-Reynolds-number Chiens (CH) $k$–$\varepsilon$ model and the low-Reynolds-number Rodi two-layer (TL) $k$–$\varepsilon$ model. Thus it is reasonable to expect improved results near the wall compared with the standard turbulence model.

In Figure 13 the velocity profiles at several positions are compared with the experimental data of Chaturvedi and the numerical profiles of Michelassi and Benocci. The comparison shows that all the methods and turbulence models are in good agreement with the experimental data.

In Figure 14 the kinetic energy profiles are plotted for the two methods. It is obvious that the axisymmetric equations provide better results than the two-dimensional equations of Michelassi and Benocci. The largest discrepancies occur near the symmetry axis and get worse

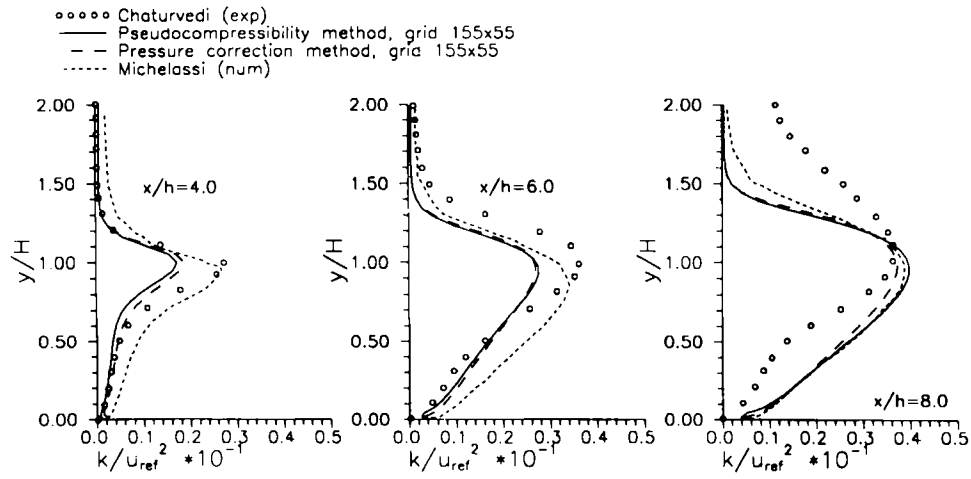


Figure 14. Kinetic energy profiles for 45° axisymmetric diffuser $Re = 2 \times 10^5$

as the exit is approached. The inadequate mesh refinement in these regions may be the main reason for the poor prediction of these profiles.

### 6.4. *Turbulent flow over a backward-facing step*

The last case investigated in the present study is the turbulent flow over a backward-facing step. Comparisons have been made with the experimental data of Kim[18] and the numerical results of Hackman *et al.*[19] The definition of the test case geometry is given in Figure 15. Selecting $u_{ref} = \bar{U}$, $L_{ref} = h$ and $\nu = \mu/\rho$, the Reynolds number becomes 69,610. In this case two grids were used, 115 × 40 and 155 × 55. In Figure 16 the 155 × 55 grid in the region around the step is shown.

In Table III a comparison of the recirculation lengths is presented. The resent results are in very good agreement with the experimental data, especially those provided by the pressure correction method. The underestimate of the recirculation length in comparison with Kim's data is a well-known property of the $k$–$\varepsilon$ turbulence model used.

Figure 17 shows the predicted pressure recovery along the lower wall of the step, starting at the root of the step, in comparison with Kim's data and other numerical results by Hackman *et al.* and Kwon and Pletcher.[20] The best behaviour is obtained by the pressure correction method.

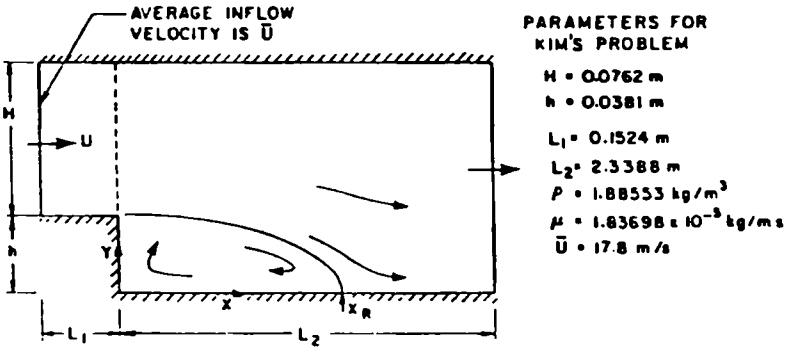


Figure 15. Definition of flow over backward-facing step

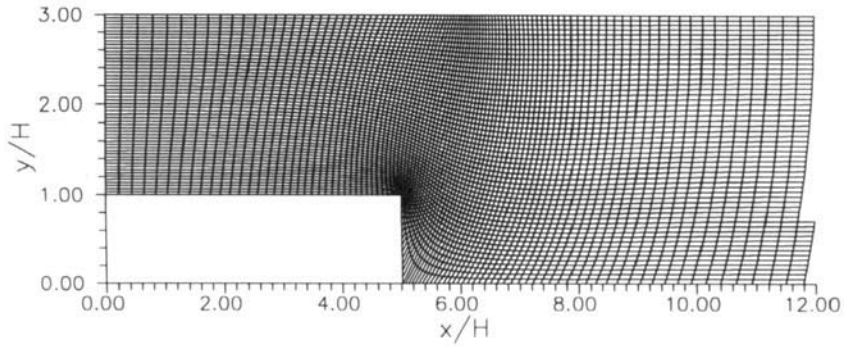


Figure 16. Detail of 155 × 55 grid in region of backward-facing step

Table III. Comparison of predicted recirculation lengths and numbers of iterations to achieve convergence for turbulent flow over a backward-facing step

| Method | Grid | Separation $x/h$ | Reattachment $x/h$ | Recirculation length | No. of iterations to $1 \times 10^{-4}$ |
|---|---|---|---|---|---|
| Experiment[18] | | | | $7{\cdot}00h \pm 0{\cdot}5h$ | |
| Pseudocompressibility | 115 × 40 | 5·00 | 11·15 | $6{\cdot}15h$ | 2829 |
| Pressure correction | 115 × 40 | 5·00 | 11·57 | $6{\cdot}57h$ | 6554 |
| Pseudocompressibility | 155 × 55 | 5·00 | 11·40 | $6{\cdot}40h$ | 4366 |
| Pressure correction | 155 × 55 | 5·00 | 11·71 | $6{\cdot}71h$ | 9682 |
| Hackman *et al.*[19] | 48 × 48 | | | $5{\cdot}2h < x < 6{\cdot}9h$ | |

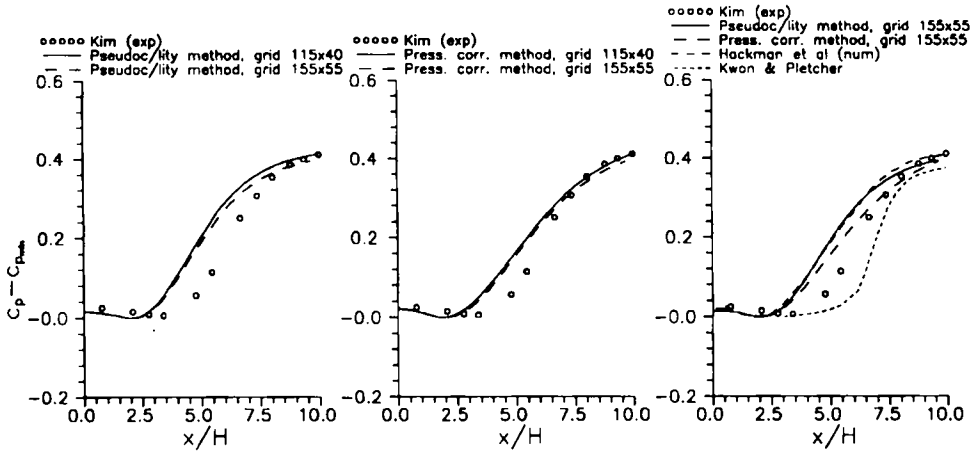


Figure 17. Predicted and measured pressure recovery $c_p - c_{min} = (p - p_{min})/(\rho u_{ref}/2)$ downstream of backward-facing step $-Re = 69{,}610$

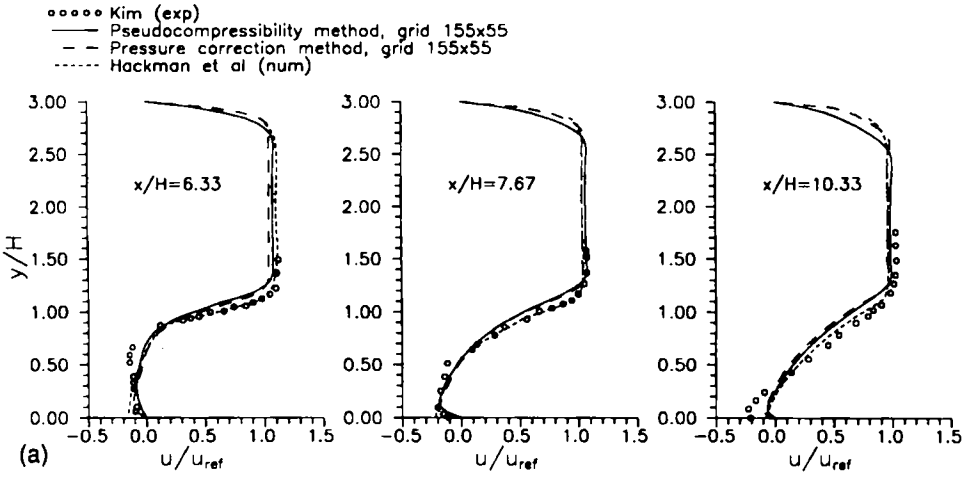


Figure 18(a). Mean velocity profiles—backward-facing step, $Re = 69{,}610$

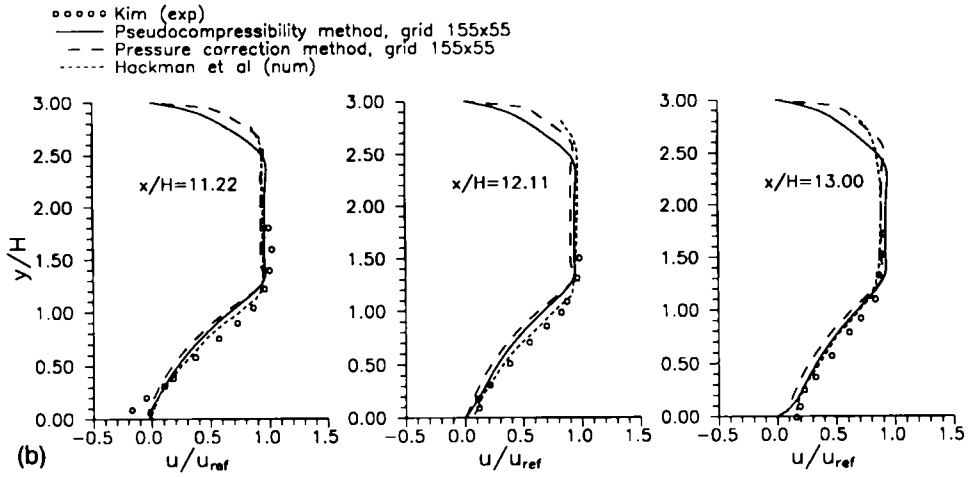


Figure 18(b). Mean velocity profiles—backward-facing step, $Re = 69{,}610$

In Figures 18(a) and 18(b) the mean velocity profiles are presented at six positions. Good agreement with the experimental results is obtained and slight differences compared with Hackman *et al.*'s results. In Figures 19(a) and 19(b) the kinetic energy profiles are shown. The comparison shows an adequate behaviour for both the two present methods and the other numerical results. Again the pressure correction method seems to have a slight superiority, Finally, in Figures 20(a) and 20(b) the convergence histories are presented for all the conservative variables. From these figures and Table III it is clear that the number of iterations the pressure correction method needs to converge is about twice the number of iterations of the pseudocompressibility method.

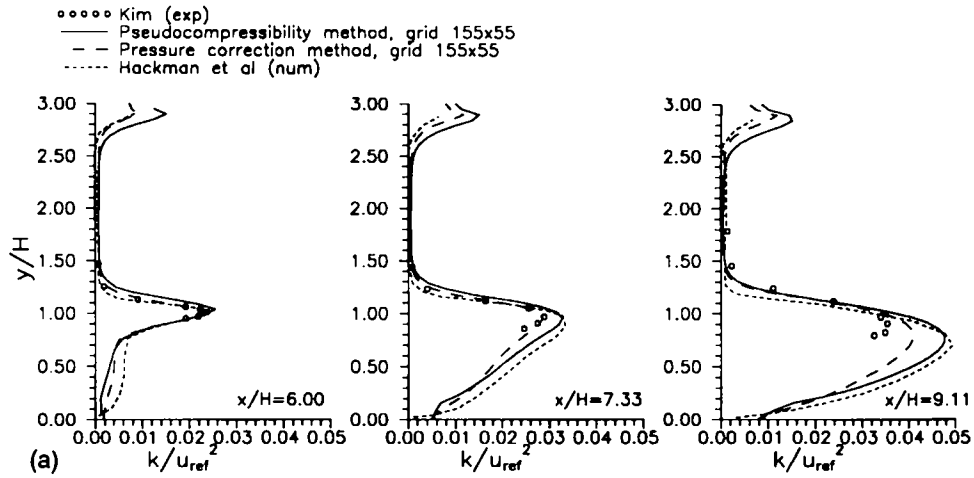


Figure 19(a). Kinetic energy profiles—backward-facing step, $Re = 69{,}610$

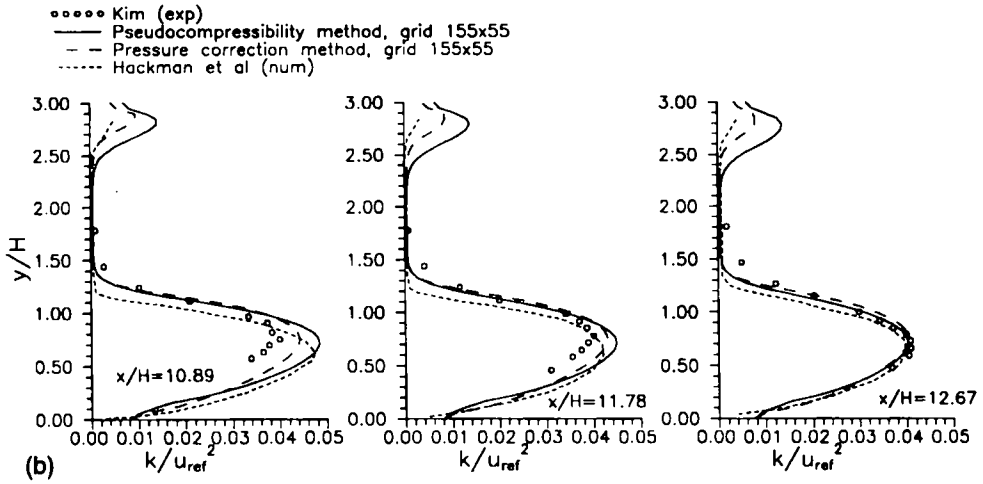


Figure 19(b). Kinetic energy profiles—backward-facing step, $Re = 69{,}610$

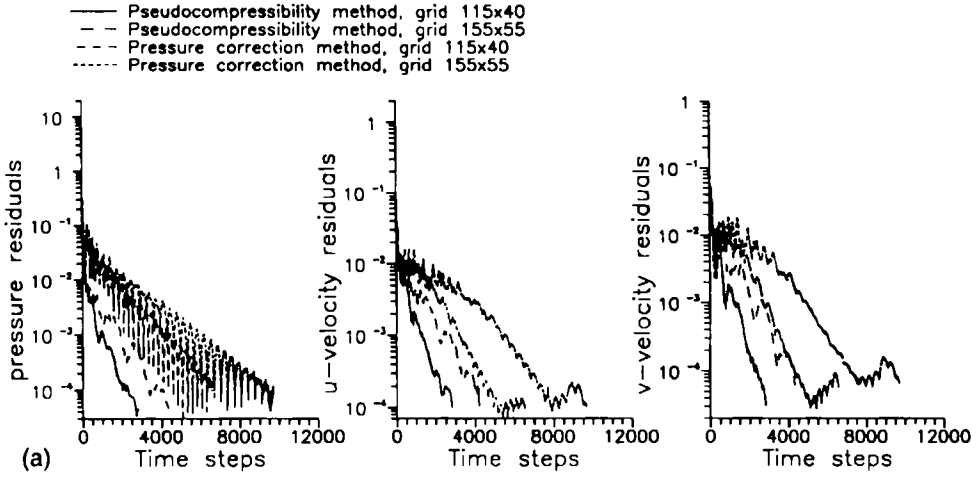


Figure 20(a). Convergence histories for pressure and velocities—backward-facing step

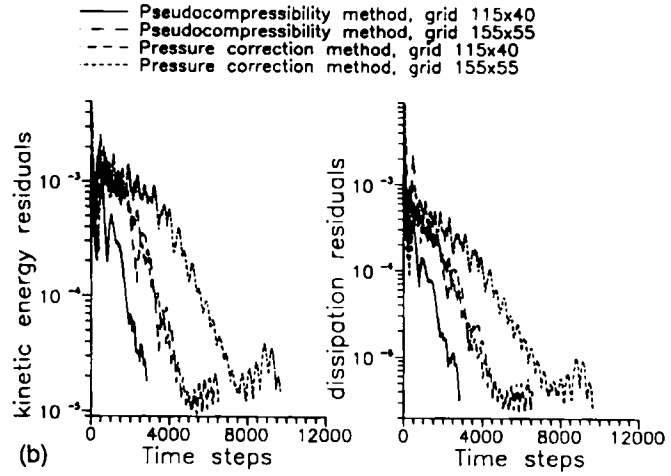


Figure 20(b). Convergence histories for kinetic energy and dissipation rate—backward-facing step

## 7. CONCLUSIONS

Two different approaches for pressure calculation and mass conservation, the artificial compressibility method and the pressure correction method, were compared in the present paper with the help of the approximate factorization technique. Several laminar and turbulent cases were used for this purpose. The standard high-Reynolds-number turbulence model was used for the turbulent flows. The comparison shows a slight superiority of the results obtained by the pressure correction method. On the other hand, the pseudocompressibility method has the advantage of much faster convergence. The use of blended second- and fourth-order artificial dissipation terms leads to excellent handling of the turbulence model equations and fast convergence of these equations is obtained.

The results in general are in very good agreement with the experimental data and in many cases are better than the corresponding numerical results of other researchers. The turbulence model could be the main reason for the discrepancies that occurred. Finally, it is noteworthy that in the axisymmetric diffuser case the recirculation region was overestimated, in contrast with the expected underestimate of this region which is the well-known behaviour of the $k$–$\varepsilon$ turbulence model.

## REFERENCES


1. R. M. Beam and R. F. Warming, 'An implicit factored scheme for the compressible Navier–Stokes equations', *AIAA J.*, **16**, 393–402 (1978).
2. V. Michelassi and C. Benocci, 'Prediction of incompressible flow separation with the approximate factorization technique', *Int. j. numer. methods fluids*, **7**, 1383–1403 (1987).
3. B. E. Launder and D. B. Spalding, 'The numerical computation of turbulent flows', *Comput. Methods Appl. Mech. Eng.*, **3**, 269–289 (1974).
4. A. J. Chorin, 'A numerical method for solving incompressible viscous flow problems', *J. Comput. Phys.*, **2**, 12–26 (1967).
5. P. Gresho, 'On the theory of semi-implicit projection methods for viscous incompressible flow and its implementation via a finite element method that also introduces a nearly consistent mass matrix. Part 1: Theory', *Int. j. numer. methods fluids*, **11**, 587–620 (1990).
6. H. I. Anderson and R. Kristoffersen, 'Numerical simulation of unsteady viscous flow', *Arch. Mech.*, **41**, 207–223 (1989).
7. S. Tsangaris, M. P. Thomadakis and A. Pentaris, 'Numerical investigation of axisymmetric compressible viscous flow', *Proc. 1st Eur. Computational Fluid Dynamics Conf.*, Brussels, 1992, pp. 835–842.
8. V. Michelassi and C. Benocci, 'Efficient solution of turbulent incompressible separated flows', *Proc. 8th GAMM Conf. on Numerical Methods in Fluid Mechanics*, (1989), Vieweg, Braunschweig, 1990, pp. 373–390.
9. A. Jameson, W. Schmidt and E. Turkel, 'Numerical solutions of the Euler equations by finite volume methods using Runge–Kutta time-stepping schemes', *AIAA Paper 81-1259*, 1981.
10. T. H. Pulliam, 'Artificial dissipation models for the Euler equations', *AIAA J.*, **24**, 1931–1940 (1986).
11. M. P. Thomadakis and S. Tsangaris, 'Improved artificial dissipation schemes for the Euler equations', *Int. j. numer. methods fluids*, **14**, 1391–1405 (1992).
12. F. Dejean, C. Vassilopoulos, G. Simandirakis, K. C. Giannakoglou and K. D. Papailiou, 'Analysis of 2-D transonic turbomachinery flows using an explicit low-Reynolds $k$–$\varepsilon$ Navier–Stokes solver', *Proc. 39th ASME Int. Gas Turbine and Aeroengine Congr. and Expos.*, The Hague, June 1994, in press.
13. D. K. Gartling, 'A test problem for outflow boundary conditions—flow over a backward-facing step', *Int. j. numer. methods fluids*, **11**, 953–967 (1990).
14. C. M. Rhie and W. L. Chow, 'Numerical study of the turbulent flow past an airfoil with trailing edge separation', *AIAA J.*, **21**, 1525–1532 (1983).
15. N. Gregory and C. L. O'Reilly, 'Low speed aerodynamic characteristics of NACA0012 airfoil section, including the effects of upper surface roughness simulation hoarfrost', *Aero Rep. 1308*, National Physical Laboratory, Teddington, 1970.
16. S. J. Shamroth and H. J. Gibeling, 'The prediction of the turbulent flow field about an isolated airfoil', *AIAA Paper 79-1543*, 1979.
17. M. C. Chaturvedi, 'Flow characteristics of axisymmetric expansions', *J. Hydraul. Div.*, 61–92 (1963).
18. J. J. Kim, 'Investigation of separation and reattachment of a turbulent shear layer: flow over a backward facing step', *Ph.D. Thesis*, Stanford University, 1978.

19. L. P. Hackman, G. D. Raithby and A. B. Strong, 'Numerical predictions on flows over backward-facing steps', *Int. j. numer. methods fluids*, **4**, 711–724 (1984).
20. O. K. Kwon and R. H. Pletcher, 'Prediction of the incompressible flow over a rearward facing step', *Tech. Rep. ISU-ERI-Ames-82019*, Engineering Research Institute, Iowa State University, Ames, IA, 1981.